Journal of Materials Science & Technology 156 (2023) 197–205

Contents lists available at ScienceDirect

Journal of Materials Science & Technology

journal homepage: www.elsevier.com/locate/jmst

Research Article

Niobium fluoride-modified hydrogen evolution reaction of magnesium borohydride diammoniate

Yujie Lv[a], Bao Zhang[b,c], Haixiang Huang[a], Bogu Liu[b], Wei Lv[b], Jianguang Yuan[b,c,*], Guanglin Xia[d], Xuebin Yu[d], Dalin Sun[d], Ying Wu[b,c,*]

[a] School of Energy Power and Mechanical Engineering, North China Electric Power University, Beijing, 102206, China
[b] Institute of Energy Power Innovation, North China Electric Power University, Beijing, 102206, China
[c] Jiangsu JITRI Advanced Energy & Materials Research Institute Co., Ltd., Changzhou, 213000, China
[d] Department of Materials Science, Fudan University, Shanghai, 200433, China

ARTICLE INFO

Article history:
Received 14 October 2022
Revised 27 December 2022
Accepted 9 January 2023
Available online 17 March 2023

Keywords:
Hydrogen storage
Magnesium borohydride
Ammoniates
NbF_5
Catalysis

ABSTRACT

Metal borohydride ammoniates have become one of the most promising hydrogen storage materials due to their ultrahigh capacities. However, their application is still restricted by the high temperature of hydrogen desorption and the release of ammonia. Here, to promote the dehydrogenation evolution and suppress the ammonia release, different amounts of NbF_5 were introduced into $Mg(BH_4)_2{\cdot}2NH_3$. Compared to the pure $Mg(BH_4)_2{\cdot}2NH_3$, the $Mg(BH_4)_2{\cdot}2NH_3$-NbF_5 composites exhibit lower onset dehydriding temperatures (53–57 °C) and higher dehydriding capacities (5.6 wt.%–8.2 wt.%) at below 200 °C, with the complete suppression of ammonia. In addition, 7.4 wt.% H_2 could be released from $Mg(BH_4)_2{\cdot}2NH_3$–5 mol% NbF_5 composite at 200 °C within 20 min and the apparent activation energy is calculated to be 60.28 kJ mol^{-1}, which is much lower than that of pure $Mg(BH_4)_2{\cdot}2NH_3$ (92.04 kJ mol^{-1}). $Mg(BH_4)_2{\cdot}2NH_3$ should mechanochemically react with NbF_5, forming dual-metal (Mg, Nb) borohydride ammoniate and spherical MgF_2. The introduction of electronegative Nb cation results *in-situ* formation of (Mg, Nb) borohydride ammoniate towards a lower dehydrogenation temperature and a higher hydrogen release purity. The increased phase boundaries among the $Mg(BH_4)_2{\cdot}2NH_3$, dual-metal (Mg, Nb) borohydride ammoniate, and MgF_2 phases further facilitate the hydrogen diffusion during the dehydrogenation of the composites.

1. Introduction

The massive use of fossil fuels such as coal and petroleum has caused serious environmental problems [1]. It is widely recognized that hydrogen, as a clean energy, is an ideal alternative to fossil fuels in the 21st century [2–4]. The development of safe, economical, and efficient hydrogen storage methods is one of the keys to the wide application of hydrogen energy [5]. In contrast with traditional methods for storing high-pressure gaseous hydrogen or low-temperature liquefied hydrogen, storing hydrogen in some solid materials such as metal hydrides and complex hydrides has been attracting considerable attention owing to their relatively safer operating conditions and higher volumetric hydrogen densities, which make solid-state hydrogen storage a most promising technology for on-board hydrogen source systems [6–9]. Magnesium borohydride ($Mg(BH_4)_2$) has great application prospects in the solid-state hydrogen storage field due to its large gravimetric hydrogen capacity of 14.9 wt.% and volumetric hydrogen density of 145–147 kg m^{-3} [10–12]. Unfortunately, the high dehydrogenation temperature, sluggish dehydrogenation kinetics, and irreversibility under mild conditions hinder its practical application. Multiple strategies have been adopted to address these disadvantages of $Mg(BH_4)_2$, mainly including doping catalysts, nanostructuring, establishing reactive systems with other hydrides, synthesizing derivatives, etc. Among these, coordinating with NH_3 to form magnesium borohydride ammoniates has been proven to be an effective strategy to improve the hydrogen desorption kinetics and lower the thermal stability of $Mg(BH_4)_2$ [13–15]. As positively charged hydrogen ($H^{\delta+}$) in NH_3 groups could combine with negatively charged hydrogen ($H^{\delta-}$) in $[BH_4]^-$ anions, and thus leads to hydrogen release of magnesium borohydride ammoniates at lower temperatures. So far, four different types of magnesium borohydride ammoniates have been reported, including $Mg(BH_4)_2{\cdot}NH_3$, $Mg(BH_4)_2{\cdot}2NH_3$, $Mg(BH_4)_2{\cdot}3NH_3$, and $Mg(BH_4)_2{\cdot}6NH_3$ [16]. $Mg(BH_4)_2{\cdot}2NH_3$ is a desirable candidate

* Corresponding authors.
E-mail addresses: yuanjianguang@atmcn.com (J. Yuan), yingwu2000@hotmail.com (Y. Wu).

https://doi.org/10.1016/j.jmst.2023.01.030
1005-0302/

for practical applications due to its large gravimetric hydrogen capacity of 16.02 wt.% and lower dehydrogenation temperature starting at around 150 °C [17]. However, the still higher dehydrogenation temperature, slower kinetics, and the hydrogen released suffering from contamination by ammonia make $Mg(BH_4)_2{\cdot}2NH_3$ unable to achieve future practical applications [18,19].

Introducing suitable additives is a commonly used method to tune the dehydriding performances of $Mg(BH_4)_2$ and its ammoniates, and fluorides have been found to exhibit superior effects in improving their dehydrogenation properties. NbF_5-doped $Mg(BH_4)_2$ has been reported to show a higher hydrogen release content and more excellent dehydriding kinetics than $Mg(BH_4)_2$ doped with the other investigated additives (*e.g.*, SiO_2, VCl_5, and $CoCl_2$) at 300 °C [20], which has been attributed to the modified dehydrogenation pathway of $Mg(BH_4)_2$ by NbF_5 with the production of MgF_2 and NbB_2 [21]. Other than group I or II halides that exhibit no obvious influence on the dehydrogenation of complex hydrides, ZnF_2 and TiF_3 could significantly decrease the onset dehydriding temperature to 50 °C, which is due to the fact that ZnF_2 or TiF_3 reacts with Mg–B–H compounds instead of playing a catalytic role [22]. Fluorographene has been found to exhibit a remarkable effect in reducing the dehydriding temperature and enhancing the dehydrogenation kinetics of the $Mg(BH_4)_2$-$NaBH_4$ composite [23] resulting from the reaction between fluorine and Mg (Na) cations. In the previous study of our team [24], $Mg(BH_4)_2$-Ti_3C_2 composites shows remarkably superior hydrogen release kinetics than that of pure $Mg(BH_4)_2$ owing to the nanoconfinement effect of Ti_3C_2 and catalysis effects of both Ti_3C_2 and fluorine on its surface. Yang *et al.* [25] introduced F into the $[BH_4]^-$ groups and prepared fluorine-substituted $Mg(BH_4)_2{\cdot}2NH_3$ by employing $LiBF_4$ as a fluorine source, and demonstrated that the fluorine-substituted $Mg(BH_4)_2{\cdot}2NH_3$ begin to desorb hydrogen at approximately 70 °C with remarkably depressed ammonia release.

Among these F-containing compounds, NbF_5 also has been utilized as an additive to several other complex hydrides and Mg-based hydrogen-storage materials to promote their hydrogenation/dehydrogenation performance [26–30]. For instance, it has been demonstrated that several transition metal (TM) fluorides could thermodynamically destabilize $NaBH_4$ and among them, the addition of NbF_5 leads to the lowest temperature for dehydrogenation [26]. TM fluorides destabilized $NaBH_4$ is affected by various factors such as the electronegativity and oxidation state of the metal, the formation enthalpy and melting point of the fluoride, etc. Cheng et al. [28] found that NbF_5 could modify the reaction pathways of the $LiBH_4{-}MgH_2{-}Al$ system, which hence results in enhanced de/rehydrogenation kinetics and superior reversibility.

Based on the above-mentioned consideration, in the present work, NbF_5 is employed as an additive to improve the hydrogen desorption reaction of $Mg(BH_4)_2{\cdot}2NH_3$ towards the enhanced dehydrogenation kinetics and the simultaneous suppression of ammonia. The mechanism of the NbF_5 additive in modifying the dehydrogenation of $Mg(BH_4)_2{\cdot}2NH_3$ is particularly studied, and the dehydriding reaction pathway of the composites is investigated as well.

2. Experimental details

2.1. Materials and general procedures

All chemical materials and the prepared samples were stored in a glove box (MBRAUN) filled with argon when not in use to prevent oxidation and dampness. O_2 and H_2O concentrations in the box were maintained at less than 0.01 ppm. The commercially purchased raw materials including sodium borohydride ($NaBH_4$, 98%, Aladdin), anhydrous magnesium chloride ($MgCl_2$, 99%, Aladdin), niobium fluoride (NbF_5, 98%, Sigma Aldrich), and ammonia gas (NH_3, 99%) were used without further processing, and anhydrous diethyl ether (AR, Sinopharm Chemical Reagent Co., Ltd.) was further dried with calcium hydride (CaH_2) before use.

2.2. Material synthesis

In diethyl ether, $Mg(BH_4)_2$ was synthesized *via* a metathesis reaction between $NaBH_4$ and $MgCl_2$ (Reaction (1)) according to a procedure that was described in our previous report [24].

$$2NaBH_4 + MgCl_2 \rightarrow Mg(BH_4)_2 + 2NaCl \quad (1)$$

Magnesium borohydride hexammoniate ($Mg(BH_4)_2{\cdot}6NH_3$) was prepared through a 24-hour ball-milling treatment of $Mg(BH_4)_2$ at 7 bar of ammonia atmosphere on a planetary ball mill (Frisch Pulverisette-6). First, 1 g $Mg(BH_4)_2$ was added to a 180 mL stainless steel milling jar in an argon-filled glove box. Then the airtight milling jar was transferred out and filled with 7 bar of ammonia using a homemade ammonification apparatus. The ammonia charging process was repeated after every 8-hour milling. The rotary velocity was 300 r min^{-1} and the ball-to-powder mass ratio was 120:1. Finally, $Mg(BH_4)_2{\cdot}6NH_3$ was obtained and collected in a glove box. Subsequently, to obtain $Mg(BH_4)_2{\cdot}2NH_3$, a mixture of 1 g $Mg(BH_4)_2{\cdot}6NH_3$ and 0.69 g $Mg(BH_4)_2$ was ball milled under 1 bar of argon atmosphere rotating at 300 r min^{-1} for 18 h. The ball-to-powder was 120:1. $Mg(BH_4)_2{\cdot}2NH_3$-$x$$NbF_5$ composites with different molar ratios (1:0.025, 1:0.05, 1:0.1, and 1:0.15) were obtained *via* ball milling the corresponding chemicals under argon atmosphere for 2 h, rotating at 300 r min^{-1}. And the ball-to-powder ratio was 40:1. To ensure the materials were uniformly mixed and ground and to prevent a temperature rise in the tank, the milling procedure was set to rotate forward for 0.2 h followed by an interruption for 0.1 h, and then a backward rotation for 0.2 h was performed. All the samples were handled in a glove box to avoid contamination from oxygen and water.

2.3. Structural and morphological characterization

The phase structures of the as-milled and the dehydrogenated samples were identified through powder X-ray diffraction (XRD, D8 Discover) with Cu K_α radiation (λ_1 = 1.54056 Å, λ_2 = 1.5444 Å) at 40 kV and 40 mA. The data were recorded from 10° to 80° (2θ) at 4° min^{-1} with a step size of 0.02° The samples were loaded in glass slides and sealed with scotch tape in an argon atmosphere to avoid rapidly oxidizing and absorbing moisture during the XRD test. Fourier transform infrared spectroscope (FTIR, Nicolet 6700 FTIR) analysis was performed to determine the vibrational characteristics of the B-H, N-H, and B-N bonds of the as-milled and dehydrogenated samples. The samples were mixed with KBr respectively (the KBr-to-sample mass ratio was 100:1) followed by tableting in a glove box. The FTIR spectra were acquired using the transmission mode with a resolution of 4 cm^{-1} between 4000 cm^{-1} and 400 cm^{-1}. To investigate the micromorphologies and surface compositions of the as-milled $Mg(BH_4)_2{\cdot}2NH_3$–5 mol% NbF_5 sample and its dehydrogenation products, a scanning electron microscope (SEM, Nova NanoSEM 450) equipped with an energy dispersive spectrometer (EDS) as well as a transmission electron microscopy (TEM, JEM-F200) was utilized. Before SEM tests, the samples were dispersed on carbon conductive tape supported on an Al holder in a glove box and then were transferred into SEM rapidly. To prepare TEM samples, some powder samples were dispersed homogeneously in anhydrous cyclohexane by ultrasonic treatment, and afterward, each suspension was dropwise added to a microgrid (200 mesh). All the treating processes were accomplished in a glove box. The samples were rapidly transferred into TEM and vacuumed before tests. The chemical valence states of

Nb in the as-milled and dehydrogenated $Mg(BH_4)_2{\cdot}2NH_3$–15 mol% NbF_5 composite were determined using X-ray photoelectron spectroscopy (XPS, Thermo Scientific K-Alpha+). A monochromatic Al K_α (1486.6 eV) X-ray source was employed to record XPS spectra under a base pressure of 5×10^{-9} mbar of air, and the analysis spot size was 400 μm in diameter.

2.4. Dehydrogenation measurement

An online mass spectrometer (MS, Hiden HPR 20) equipped with temperature-programmed desorption (TPD) apparatus was used for determining the multi-step desorption temperatures of the as-prepared samples. Under a nitrogen flow of 50 mL min^{-1}, each sample weighing ~20 mg was heated at a heating rate of 2 °C min^{-1} from room temperature (RT) to 500 °C in a specially designed tubular reactor and the gasses released were detected in real-time.

A homemade Sieverts-type apparatus was employed to measure the dehydriding properties of the as-prepared samples using the volumetric method. For each test, ~100 mg powder was sealed in a stainless steel tubular reactor under an argon atmosphere. The reactor was connected to the Sieverts-type apparatus and vacuumed and heated from RT to 350 °C at a rate of 2 °C min^{-1}. The changes in system pressure and sample temperature were automatically recorded and subsequently utilized to analyze the released hydrogen amount according to the ideal gas state equation. An isothermal dehydrogenation test at different temperatures was further carried out for the composite with the optimal NbF_5 content. And then the dehydrogenation apparent activation energy (E_a) was calculated on the base of Arrhenius formula [31,32].

3. Results and discussion

By mixing $Mg(BH_4)_2{\cdot}2NH_3$ and NbF_5 with different molar ratios *via* mechanical milling, four $Mg(BH_4)_2{\cdot}2NH_3$-*x*NbF_5 (x = 2.5 mol%, 5 mol%, 10 mol%, and 15 mol%) samples were synthesized. A slight pressure increase is detected in each milling jar containing the $Mg(BH_4)_2{\cdot}2NH_3$-NbF_5 mixture after the ball milling process. Mass (MS) full-spectrum analysis of gas composition in the jar containing the milled $Mg(BH_4)_2{\cdot}2NH_3$–5 mol% NbF_5 composite reveals that only hydrogen is released during the ball milling process (Fig. S1, Supporting Information). This result indicates that NbF_5 could effectively destabilize $Mg(BH_4)_2{\cdot}2NH_3$, resulting in the release of a small amount of hydrogen during the milling process.

Fig. 1 shows the X-ray diffraction (XRD) patterns and Fourier transform infrared (FTIR) spectra of the as-milled $Mg(BH_4)_2{\cdot}2NH_3$-*x*NbF_5 samples. For comparison, the corresponding results of the pristine $Mg(BH_4)_2{\cdot}2NH_3$ and NbF_5 processed under the same conditions are also displayed. XRD profile (Fig. 1(a)) of the as-synthesized $Mg(BH_4)_2{\cdot}2NH_3$ displays twelve obvious peaks at 14.7°, 17.1°, 18.8°, 20.2°, 22.0°, 24.3°, 26.3°, 27.8°, 29.0°, 31.8°, 33.7°, and 39.9° (2θ), which matches well with the XRD pattern of $Mg(BH_4)_2{\cdot}2NH_3$ reported by Soloveichik *et al.* [33], representing the successful preparation of $Mg(BH_4)_2{\cdot}2NH_3$ in this study. After the addition of 2.5 mol% and 5 mol% NbF_5, only diffraction peaks of $Mg(BH_4)_2{\cdot}2NH_3$ phase are displayed in the XRD profile and their peak intensities are obviously weakened compared with that of pure $Mg(BH_4)_2{\cdot}2NH_3$. As the NbF_5 content increases to 10 mol%, the peak intensities of the $Mg(BH_4)_2{\cdot}2NH_3$ phase further decrease and a new diffraction peak appears at 16.6° Severe amorphization is observed in the $Mg(BH_4)_2{\cdot}2NH_3$–15 mol% NbF_5 composite with the observation of only a few weak diffraction peaks of $Mg(BH_4)_2{\cdot}2NH_3$ and some newly emerged peaks. However, those new peaks are unidentifiable and do not belong to any known phases. High-resolution Nb 3d X-ray photoelectron spectroscopy (XPS) result of the as-milled $Mg(BH_4)_2{\cdot}2NH_3$–15 mol% NbF_5 composite (Fig. S2) shows that niobium is in Nb^{5+} and Nb^{2+} valence states. However, the binding energy (BE) peaks of Nb^{5+} 3d in the composite are nearly 2.7 eV lower than that of Nb^{5+} 3d in NbF_5, which indicates the formation of a different Nb^{5+}-containing compound. Moreover, the dehydrogenation during ball milling leads to a decrease in the valence of Nb from +5 to +2. The XRD and XPS results indicate that $Mg(BH_4)_2{\cdot}2NH_3$ reacts with NbF_5 during milling.

FTIR examinations of the as-milled $Mg(BH_4)_2{\cdot}2NH_3$ and the NbF_5-doped composites were conducted to characterize the B-H and N-H vibrations (Fig. 1(b)). The relevant absorption bands acquired from the FTIR spectra are listed in Table 1. As for pure $Mg(BH_4)_2{\cdot}2NH_3$, the typical absorbance peaks of N-H stretching vibrations are observed at 3353–3208 cm^{-1}, and an N-H bending vibration at 1608 cm^{-1} is detected. The absorbance bands at 2343–2222 cm^{-1} and 1234–1123 cm^{-1} are associated with the stretching and bending vibrations of B-H, respectively. After introducing NbF_5, similar B-H and N-H vibrations are detected in all the $Mg(BH_4)_2{\cdot}2NH_3$-NbF_5 composites. No Nb-F and B-F vibrations are detected. However, an absorbance peak corresponding to N-H vibration (3208 cm^{-1}) could not be detected in the FTIR spectra of the $Mg(BH_4)_2{\cdot}2NH_3$-*x*NbF_5 (x = 5 mol%, 10 mol%, 15 mol%) composites. In addition, blue shifts are observed for the B-H stretching vibrations of the $Mg(BH_4)_2{\cdot}2NH_3$-*x*NbF_5 (x = 2.5 mol%, 5 mol%) composites, while redshifts occur in the counterparts of the 10 mol% and 15 mol% NbF_5-doped $Mg(BH_4)_2{\cdot}2NH_3$. The shifts of the B-H absorption peaks show no obvious rules. According to these results, the chemical environments of N, B, and H are altered by the addition of NbF_5.

The above analyses demonstrate that $Mg(BH_4)_2{\cdot}2NH_3$-NbF_5 is a reactive system. Metal borohydride ammoniate is the main component in all the as-milled $Mg(BH_4)_2{\cdot}2NH_3$-NbF_5 composites. Some dual-metal borohydride ammoniates such as $VMg(BH_4)_5{\cdot}5NH_3$, $Li_2Mg(BH_4)_4{\cdot}6NH_3$, and $Mg_{0.5}Mn_{0.5}(BH_4)_2{\cdot}6NH_3$ have been reported [34–36]. In this study, it could be deduced that after ball milling the reaction products of $Mg(BH_4)_2{\cdot}2NH_3$ with NbF_5 are a new kind of dual-metal (Mg, Nb) borohydride ammoniate and MgF_2. The unassigned Bragg peaks, such as 15.7° and 16.6° in the XRD patterns of the 10 mol% and 15 mol% NbF_5-doped samples are assumed to belong to the dual-metal (Mg, Nb) borohydride ammoniate phase, while MgF_2 shows amorphous.

The temperature-programmed desorption-mass spectrometer (TPD-MS) results of the as-milled $Mg(BH_4)_2{\cdot}2NH_3$ and its NbF_5-doped composites are shown in Fig. 2. Both the samples present multi-step thermal decomposition processes at RT~500 °C. For the pure $Mg(BH_4)_2{\cdot}2NH_3$, there are three main hydrogen release peaks located at 207 °C, 225 °C, and 403 °C, respectively, with an onset dehydrogenation temperature (T_{onset}) at 123 °C, and NH_3 is detected in the temperature range of 110–260 °C upon decomposition. As NbF_5 is introduced, the $Mg(BH_4)_2{\cdot}2NH_3$-NbF_5 composites could start hydrogen evolution at a temperature as low as 53–57 °C. For the composite doped with 2.5 mol% NbF_5, an additional subtle hydrogen release process is observed at 53–103 °C, indicating a more complicated multistep decomposition pathway. The most intensive dehydrogenation peak is reduced from 207 °C for $Mg(BH_4)_2{\cdot}2NH_3$ to 183 °C, while the last peak increases to 422 °C. The results suggest an enhanced hydrogen release kinetics for the 2.5 mol% NbF_5-doped composite compared to the pristine $Mg(BH_4)_2{\cdot}2NH_3$. When the NbF_5 amount increases to 5 mol%, the most intensive dehydrogenation peak is reduced to 171 °C, and the last peak increases to 441 °C. As for $Mg(BH_4)_2{\cdot}2NH_3$ added with 10 mol% and 15 mol% NbF_5 respectively, the hydrogen release peaks in the temperature range of 54–107 °C show gradually increased intensities, and ultimately dominate the MS curve of the 15 mol% NbF_5-containing composite. However, no dehydrid-

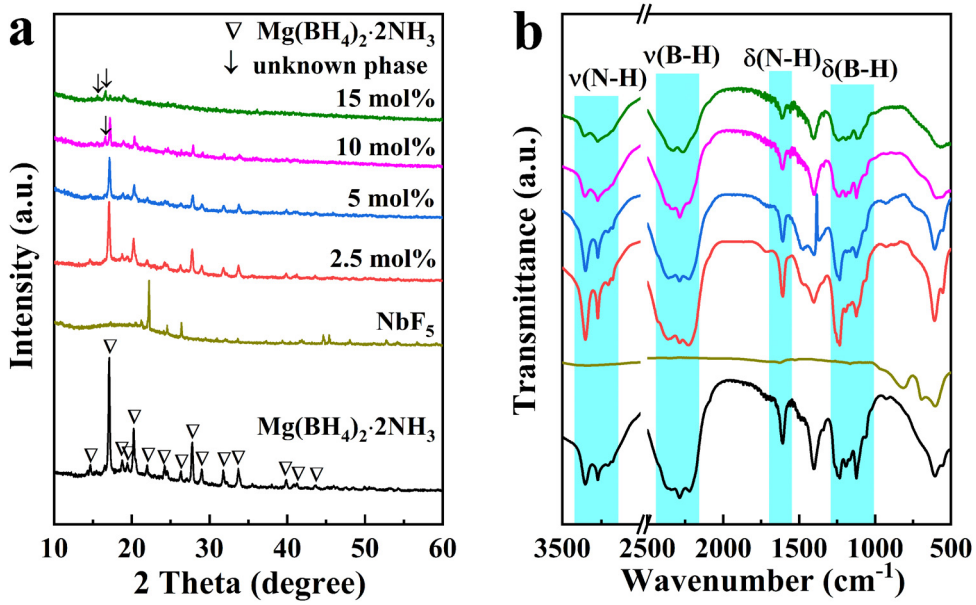

Fig. 1. (a) XRD patterns and (b) FTIR spectra of the as-prepared $Mg(BH_4)_2·2NH_3$-NbF_5 composites with different NbF_5 contents.

Table 1
Absorption bands (in cm^{-1}) of the as-milled $Mg(BH_4)_2·2NH_3$ and $Mg(BH_4)_2·2NH_3$-$x$$NbF_5$ (x = 2.5 mol%, 5 mol%, 10 mol%, 15 mol%) composites.

Samples	ν(N-H)	ν(B-H)	δ(N-H)	δ(B-H)
$Mg(BH_4)_2·2NH_3$	3353, 3274, 3208	2343, 2288, 2222	1608	1234, 1193, 1169, 1123
x = 2.5	3354, 3273, 3208	2363, 2288, 2226	1609	1234, 1194, –, 1125
x = 5	3352, 3273, –	2359, 2289, 2226	1609	1234, 1185, 1167, 1125
x = 10	3356, 3274, –	2331, 2287, 2225	1608	1234, 1193, 1169, 1123
x = 15	3357, 3274, –	2330, 2267, –	1609	1239, 1193, 1169, 1120

ν: Stretching mode, δ: Bending mode.

ing peak could be observed from 400 °C to 500 °C. As reported by Yang et al. [17], MgH_2 is an intermediate decomposition product of $Mg(BH_4)_2·2NH_3$, and the dehydrogenation peak above 400 °C in the TPD-MS profile of $Mg(BH_4)_2·2NH_3$ is similar to the MS desorption peak of MgH_2. In the present work, the dehydrogenation behavior of $Mg(BH_4)_2·2NH_3$ between 390 °C and 450 °C is attributed to the decomposition of MgH_2. As NbF_5 is introduced to $Mg(BH_4)_2·2NH_3$, part of Mg ions exist in MgF_2 after milling treatment, and the proportion of Mg in the borohydride ammoniates reduces simultaneously. Thus the formation of MgH_2 is also reduced in the thermal decomposition process. This effect is more remarkable in the 10 mol% and 15 mol% NbF_5-doped composites, which contributes to the disappearance of the MS dehydrogenation peak at 400–500 °C. Furthermore, it should be noted that the ammonia released is greatly inhibited and no other gas by-products such as B_2H_6 and HF are released for all the $Mg(BH_4)_2·2NH_3$-NbF_5 systems. The TPD-MS results show that the introduction of NbF_5 into $Mg(BH_4)_2·2NH_3$ could simultaneously reduce the hydrogen desorption temperature and inhibit ammonia release.

Volumetric hydrogen release curves of the as-prepared $Mg(BH_4)_2·2NH_3$ and $Mg(BH_4)_2·2NH_3$-$x$$NbF_5$ samples were measured from RT to 350 °C to quantitatively investigate their dehydrogenation behavior. Fig. 3(a) displays that the pristine $Mg(BH_4)_2·2NH_3$ starts releasing H_2 from 123 °C and desorbs a total of 11.9 wt.% H_2 when heated to 350 °C, which is in accordance with Refs. [16,25]. After introducing NbF_5, the initial hydrogen release temperatures of the samples reduce to 53–57 °C, and the hydrogen desorption contents up to 350 °C amount to 12.2 wt.%, 12.4 wt.%, 10.9 wt.%, and 10.1 wt.% for the samples with NbF_5 additive amounts of 2.5 mol%, 5 mol%, 10 mol%, and 15 mol%, respectively. Fig. 3(b) shows that when NbF_5 content increases, the $Mg(BH_4)_2·2NH_3$-$x$$NbF_5$ composites release H_2 with a gradually increased proportion of the corresponding theoretical hydrogen contents at relatively low temperatures such as 150 °C and 200 °C. The above results match well with those of MS tests and indicate the excellent modification effect of NbF_5 on the dehydriding kinetics of $Mg(BH_4)_2·2NH_3$. The higher content of NbF_5 exhibits a more stimulation effect, although resulting in a reduction of total hydrogen capacity. $Mg(BH_4)_2·2NH_3$–5 mol% NbF_5 composite possesses the optimal comprehensive dehydrogenation properties when dehydriding kinetics and hydrogen release content are considered together. It starts to release hydrogen at 57 °C and desorbs 8.2 wt.% H_2 when the temperature rises to 200 °C, which is 56.3% of its theoretical hydrogen capacity. However, only 2.2 wt.% H_2 could the pure $Mg(BH_4)_2·2NH_3$ release in the same condition, and the corresponding hydrogen release ratio is 13.7%.

To further evaluate the effect of NbF_5 in enhancing the dehydriding kinetics of $Mg(BH_4)_2·2NH_3$, isothermal dehydrogenation tests were carried out at various temperatures with the calculation of their dehydrogenation apparent activation energies (E_a) based on Arrhenius formula. As illustrated in Fig. 4(a, b), the as-milled $Mg(BH_4)_2·2NH_3$–5 mol% NbF_5 composite exhibits more excellent hydrogen evolution kinetics than the pure $Mg(BH_4)_2·2NH_3$ that it desorbs 7.4 wt.% H_2 at 200 °C within just 20 min. Even when the temperature decreases to 160 °C, 5.9 wt.% H_2 could be released from the composite within 120 min. However, the pure $Mg(BH_4)_2·2NH_3$ releases only 2.6 wt.% H_2 at 160 °C and 6.5 wt.% at even 220 °C over 120 min, suggesting slower dehydriding rates. The same dehydriding capacities could be achieved within 21 min and 7 min, respectively, at the corresponding temperatures for

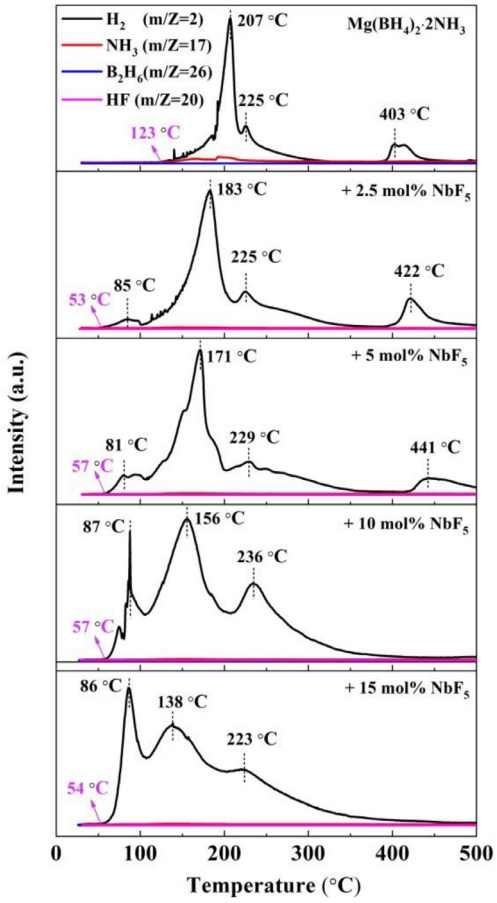

Fig. 2. TPD-MS profiles of the as-prepared $Mg(BH_4)_2{\cdot}2NH_3$ and $Mg(BH_4)_2{\cdot}2NH_3$-$x$$NbF_5$ composites from room temperature to 500 °C at a heating rate of 2 °C min^{-1}.

the $Mg(BH_4)_2{\cdot}2NH_3$–5 mol% NbF_5 composite. The dehydrogenation apparent activation energies of the two samples are calculated using their isothermal dehydrogenation data at different temperatures [31,32]. By plotting Arrhenius profiles of the dehydrogenation kinetics and linear fitting, the E_a values of the pristine $Mg(BH_4)_2{\cdot}2NH_3$ and the 5 mol% NbF_5-doped composite are calculated to be 92.04 kJ mol^{-1} and 60.28 kJ mol^{-1}, respectively. A remarkable reduction of 31.76 kJ mol^{-1} for the E_a of the 5 mol% NbF_5-doped composite further confirms that the dehydrogenation kinetics of $Mg(BH_4)_2{\cdot}2NH_3$ could be significantly enhanced by the introduction of NbF_5.

To understand the dehydrogenation mechanisms of $Mg(BH_4)_2{\cdot}2NH_3$ and the NbF_5-doped composites, XRD and FTIR tests were conducted on their dehydrogenated products at 500 °C. As shown in Fig. 5(a), after $Mg(BH_4)_2{\cdot}2NH_3$ and the 2.5 mol% NbF_5-doped composite are heated to 500 °C, several obvious diffraction peaks at 32.1°, 34.3°, 36.6°, 47.7°, 57.3°, 63.1°, 68.6°, and 69.9°, respectively, are observed in the XRD patterns of their decomposition products. Those peaks are assigned to the Mg phase (PDF# 35–0821). In addition, a diffuse diffraction peak at 40°–45° (2θ) could be assigned to boron nitride (BN) according to the previous reports [17,37]. Several additional weak peaks of the MgF_2 phase (PDF# 41–1443) at 27.3°, 40.4°, and 53.5° are detected by XRD in the decomposition product of the 5 mol% NbF_5-doped samples. However, the amorphous character of the dehydrogenated 10 mol% and 15 mol% NbF_5-containing samples becomes more obvious with the increase of NbF_5 content, and only weak characteristic peaks of BN and MgF_2 could be identified. As shown in the FTIR spectra (Fig. 5(b)) of the five dehydrogenated samples, the absorbance peaks at 1375 cm^{-1} and 1135 cm^{-1} assigned to ν(B-N), and 799 cm^{-1} assigned to δ(B-N) are observed, which correspond to the B-N bands of BN. The disappearance of B-H and N-H absorbance peaks indicates adequate dehydrogenation for the samples at 500 °C. Combining XRD and FTIR analyses of the as-milled and dehydrogenated samples, it could be concluded that 1) dual-metal (Mg, Nb) borohydride ammoniate and MgF_2 generate during the balling milling process between $Mg(BH_4)_2{\cdot}2NH_3$ and NbF_5; 2) upon heating, the interaction between $H^{\delta+}$ and $H^{\delta-}$ in the dual-metal (Mg, Nb) borohydride ammoniate and $Mg(BH_4)_2{\cdot}2NH_3$ liberates H_2 by generating Mg and BN in the thermal decomposition process ultimately. However, no phase containing Nb element is detected by the XRD tests on the dehydrogenated NbF_5-containing samples.

The 5 mol% NbF_5-doped sample was chosen as a representative of the $Mg(BH_4)_2{\cdot}2NH_3$-NbF_5 composites and its changes in microstructure as well as phase structure after thermal decomposition at 500 °C were investigated. Scanning electron microscope (SEM) images of the as-milled $Mg(BH_4)_2{\cdot}2NH_3$–5 mol% NbF_5 composite and its dehydrogenation products at 500 °C together with element mappings are shown in Fig. 6(a–e). As shown in (Fig. 6(a)), the 5 mol% NbF_5-doped composite powder has an irregular particle shape and uneven size distribution (from a few microns to dozens of micron range). The corresponding element mapping result (Fig. S3) indicates that F and Nb are evenly distributed in the 5 mol% NbF_5-doped sample. Interestingly, particles with two morphologies are observed in the dehydrogenation product (Fig. 6(b)). A kind of irregularly shaped particle is found to vary in size from a few microns to a few hundred microns, in which some holes of different sizes are distributed, possibly due to gas release when heat-

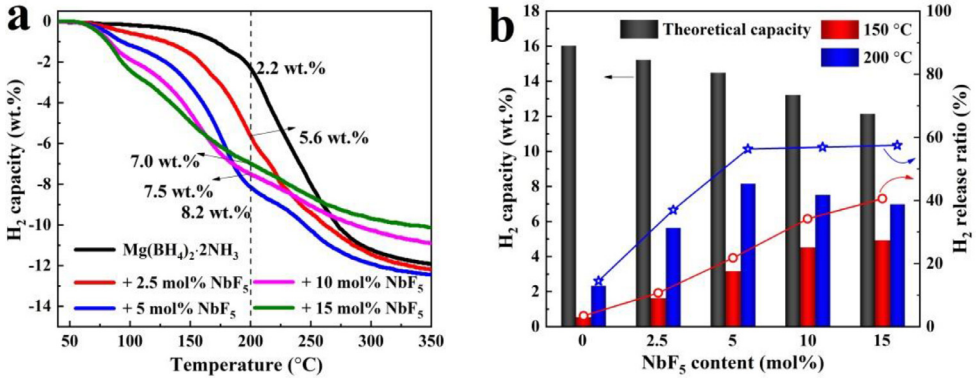

Fig. 3. (a) Volumetric release curves of the as-prepared $Mg(BH_4)_2{\cdot}2NH_3$ and $Mg(BH_4)_2{\cdot}2NH_3$-x NbF_5 (x = 2.5 mol%, 5 mol%, 10 mol%, and 15 mol%) composites from room temperature to 350 °C at a heating rate of 2 °C min^{-1} under an initial hydrogen pressure of 10^{-3} bar and (b) the summary of hydrogen release at different temperatures.

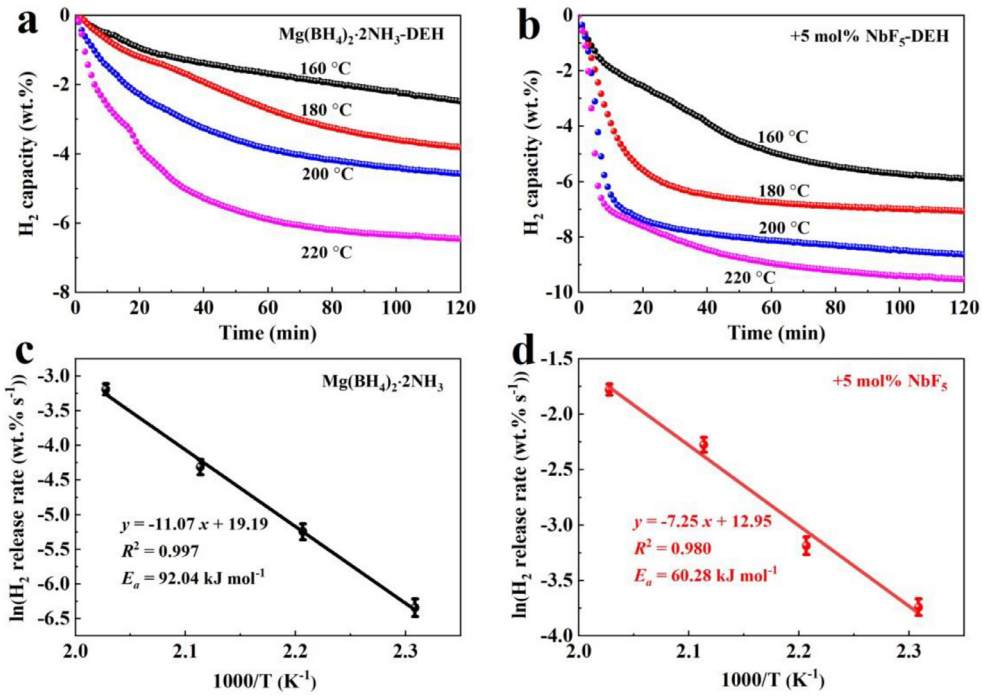

Fig. 4. The isothermal dehydrogenation curves of (a) the as-prepared $Mg(BH_4)_2{\cdot}2NH_3$ and (b) $Mg(BH_4)_2{\cdot}2NH_3$–5 mol% NbF_5 composite at different temperatures. (c) and (d) Arrhenius plots of the two samples.

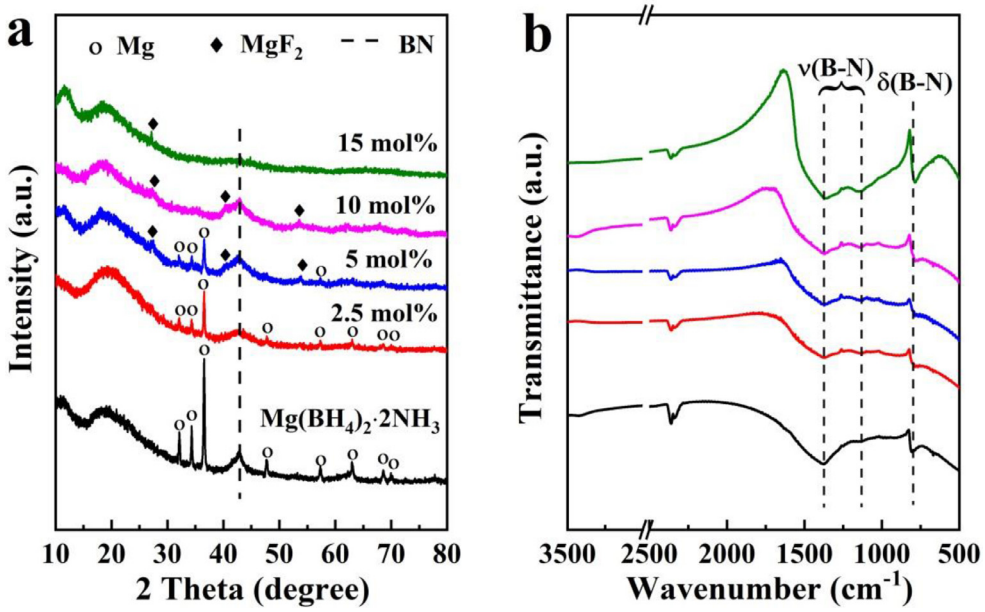

Fig. 5. (a) XRD patterns and (b) FTIR spectra of the dehydrogenated $Mg(BH_4)_2{\cdot}2NH_3$-NbF_5 composites with different NbF_5 contents at 500 °C.

ing. Another kind of particle that is close to spherical with several micron diameters could be observed attaching to the former particles. The special morphology is shown in detail by a further magnified SEM image (Fig. 6(c)) of the dehydrogenated 5 mol% NbF_5-containing composite. The corresponding elemental mapping displays that B, N, and Nb elements are mainly enriched in the particles with multi-hole structure, while those near-spheroidal particles contain higher Mg and F contents. Fig. 6(d, e) is the transmission electron microscopy (TEM) image of the dehydrogenated 5 mol% NbF_5-containing composite at 500 °C and the corresponding selected area electron diffraction (SAED) pattern. The phase identification and the corresponding crystal planes are stated in Fig. 6(e). Mg, MgF_2, and NbH phases are determined in the micro-area that is displayed in Fig. 6(d).

XPS analysis was also applied to the dehydrogenated $Mg(BH_4)_2{\cdot}2NH_3$–15 mol% NbF_5 at 500 °C to trace the Nb element. The XPS spectrum of Nb 3d (Fig. S4) shows two peaks centered at 203.4 eV and 206.1 eV corresponding to the Nb^+ $3d_{5/2}$ and Nb^+ $3d_{3/2}$ levels in NbH [38], which is consistent with the above SAED result. These analyses reveal that Nb element exists as the only form of NbH in the dehydrogenated NbF_5-containing composite at 500 °C.

Fig. 7 illustrates the reaction paths and dehydrogenation mechanism of the $Mg(BH_4)_2{\cdot}2NH_3$-NbF_5 composites based on the above

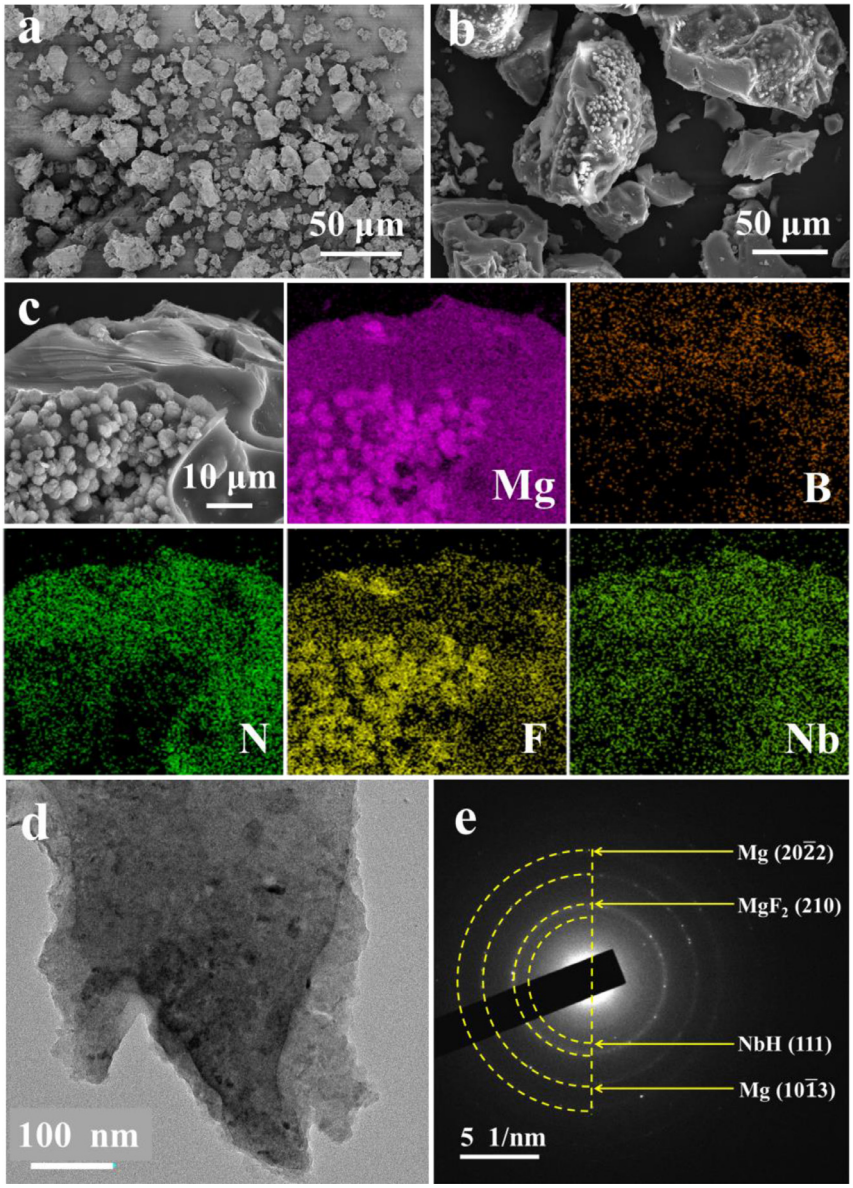

Fig. 6. SEM images of (a) the as-milled $Mg(BH_4)_2{\cdot}2NH_3$–5 mol% NbF_5, (b) the dehydrogenated $Mg(BH_4)_2{\cdot}2NH_3$–5 mol% NbF_5 composite at 500 °C, (c) element mapping of the dehydrogenated $Mg(BH_4)_2{\cdot}2NH_3$–5 mol% NbF_5 composite. (d) TEM image, and (e) the corresponding SAED pattern of the dehydrogenated $Mg(BH_4)_2{\cdot}2NH_3$–5 mol% NbF_5 composite at 500 °C.

analyses. The phase transition during ball milling and the thermal decomposition reaction could be described as follows:

$$6Mg(BH_4)_2 \cdot 2NH_3 + 2NbF_5 \xrightarrow{\text{ball milling for 2 h}} (Mg, Nb) \times \text{borohydride ammoniates} + 5MgF_2 \quad (2)$$

$$(Mg, Nb)\ \text{borohydride ammoniates} + 5MgF_2 \xrightarrow{RT-500\ ^\circ C} Mg + 5MgF_2 + 12BN + 2NbH + 41H_2 \uparrow \quad (3)$$

After ball milling, there are $Mg(BH_4)_2{\cdot}2NH_3$, dual-metal (Mg, Nb) borohydride ammoniate, and MgF_2 in the as-milled NbF_5-containing composites. Previous theoretical and experimental studies have revealed that the metal cations (M) of $M(BH_4)_n{\cdot}mNH_3$ play an important role in facilitating the combination of N-H and B-H bonds during their dehydrogenation evolutions [39–42]. $M(BH_4)_n{\cdot}mNH_3$ in which the metal ions that have the higher Pauling electronegativity (χ_p) values show lower hydrogen release temperatures [39,40]. Therefore, introducing metal cations with higher χ_p values to form multiple-cation borohydride ammoniates could be effective to improve their hydrogen desorption properties. The χ_p value of Nb (1.6) is higher than that of Mg (1.31). Thus in this study, the formation of dual-metal (Mg, Nb) borohydride ammoniate during milling decreases the dehydrogenation temperatures and improves the dehydriding kinetics of the $Mg(BH_4)_2{\cdot}2NH_3$-NbF_5 composites. Furthermore, the increased number of phase boundaries between the $Mg(BH_4)_2{\cdot}2NH_3$, dual-metal (Mg, Nb) borohydride ammoniate and MgF_2 phases in the as-milled composites could serve as hydrogen diffusion channels and thus enhance the dehydrogenation kinetics as well [43,44]. Some studies have suggested that it exists a competitive relationship between the combination of $H^{\delta+}$-$H^{\delta-}$ and the breaking of N:→Mg^{2+} coordination bonds processes [16,25], and the latter process leads to ammonia release. Therefore, when the hydrogen release resulting from the combination of $H^{\delta+}$ and $H^{\delta-}$ is promoted with the formation of dual-metal (Mg, Nb) borohydride ammoniate, ammonia release will also be inhibited in the $Mg(BH_4)_2{\cdot}2NH_3$-NbF_5 system.

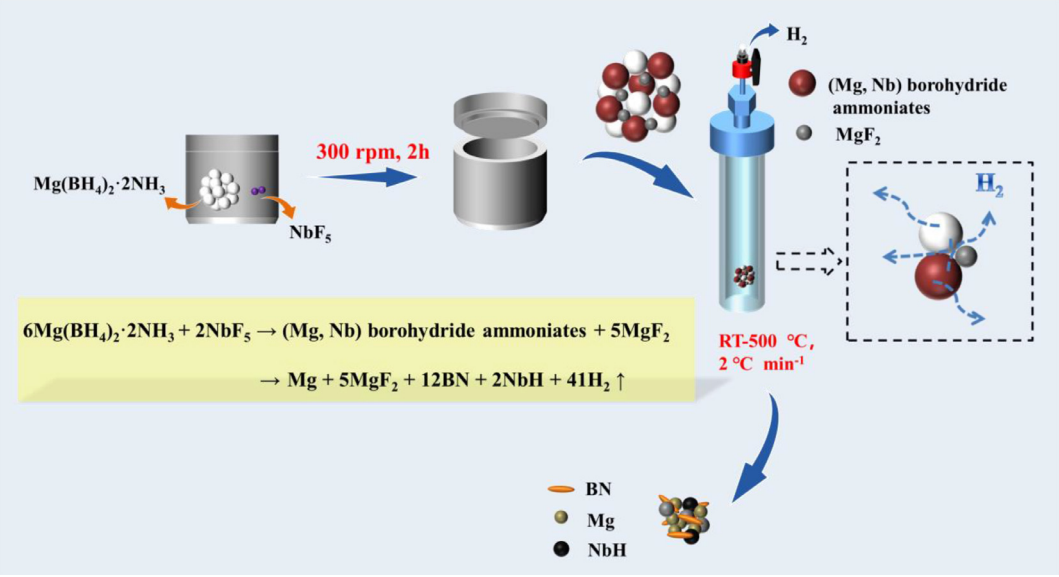

Fig. 7. Reaction paths and dehydrogenation mechanism of the $Mg(BH_4)_2·2NH_3$-NbF_5 composites.

It is worth noting that the decomposition product of the $Mg(BH_4)_2·2NH_3$–5 mol% NbF_5 composite after sufficient dehydrogenation at 500 °C could absorb and desorb hydrogen reversibly (Fig. S5). The dehydrogenated $Mg(BH_4)_2·2NH_3$–5 mol% NbF_5 composite was first hydrogenated at 400 °C under 10 MPa H_2 pressure for 6 h and followed by dehydriding from RT to 500 °C with varying heating rates. The hydrogenated sample starts to release hydrogen at about 170 °C and desorbs 5.1 wt.% in total until 500 °C, exhibiting excellent reversibility. The XRD pattern and the FTIR spectrum of the rehydrogenation product were tested. As shown in Fig. S6, BN, MgF_2, and MgO phases are detected by XRD, with no crystalline Mg and Nb-containing phases observed. However, the MgH_2 phase is not detected as well, indicating that MgH_2 is not the final hydrogenation product. The FTIR spectrum (Fig. S7) displays the absorbance peaks of B-H and B-N stretching and bending vibrations. Therefore, hydrogen is believed to reversibly store in the borohydride of Mg (and/or Nb).

4. Conclusions

In summary, a new $Mg(BH_4)_2·2NH_3$-based hydrogen storage material system is synthesized with the introduction of NbF_5 by ball-milling, which shows significantly enhanced dehydrogenation kinetics properties and greatly inhibited ammonia release. The T_{onset} is remarkably reduced to 53–57 °C for the $Mg(BH_4)_2·2NH_3$-NbF_5 composites, and 10.1 wt.%–12.4 wt.% hydrogen could be desorbed under 350 °C. The $Mg(BH_4)_2·2NH_3$–5 mol% NbF_5 composite exhibits the best comprehensive dehydrogenation properties. It could release 8.2 wt.% pure H_2 when heated to 200 °C, which is almost 3.7 times higher than that of the pristine $Mg(BH_4)_2·2NH_3$. The E_a of the $Mg(BH_4)_2·2NH_3$–5 mol% NbF_5 composite is 60.28 kJ mol^{-1}, which is 31.76 kJ mol^{-1} lower than that of $Mg(BH_4)_2·2NH_3$, indicating the superior dehydriding kinetics due to NbF_5. The highly improved dehydrogenation performance is mainly attributed to the *in-situ* formation of dual-metal (Mg, Nb) borohydride ammoniate with lower stability through the mechanochemical reaction between $Mg(BH_4)_2·2NH_3$ and NbF_5. In addition, the increase of phase boundaries due to the newly generated (Mg, Nb) borohydride ammoniate and MgF_2 phases provide more hydrogen diffusion channels during the dehydrogenation process, which further facilitates hydrogen release. The lowered operating temperature and high hydrogen release purity of the $Mg(BH_4)_2·2NH_3$-NbF_5 system make it a great potential hydrogen storage material for onboard applications.

Acknowledgments

This work was supported by the National Key Research and Development Plan (Grant No. 2021YFB3802400), the National Natural Science Foundation of China (Grant Nos. 52071141, 52271212, 52201250), the Equipment Pre-research Field Foundation (Grant No. 6140721040101), and the Inter-disciplinary Innovation Program of North China Electric Power University (Grant No. XM2112355).

Supplementary materials

Supplementary material associated with this article can be found, in the online version, at doi:10.1016/j.jmst.2023.01.030.

References

[1] G.H. Liu, L.X. Wang, Y. Hu, C.H. Sun, H.Y. Leng, Q. L, C.Z. Wu, J. Alloy. Compd. 881 (2021) 160644.
[2] W. Chen, L. You, G.L. Xia, X.B. Yu, J. Mater. Sci. Technol. 79 (2021) 205–211.
[3] S. Wei, J.X. Liu, Y.P. Xia, H.Z. Zhang, R.G. Cheng, L.X. Sun, F. Xu, P.R. Huang, F. Rosei, A.A. Pimerzin, H.J. Seifert, H.G. Pan, J. Mater. Sci. Technol. 111 (2022) 189–203.
[4] W.S. Ko, K.B. Park, H.Ki Park, J. Mater. Sci. Technol. 92 (2021) 148–158.
[5] Y.P. Pang, Q. Li, Scr. Mater. 130 (2017) 223–228.
[6] X.B. Yu, Z.W. Tang, D.L. Sun, L.Z. Ouyang, M. Zhu, Prog. Mater. Sci. 88 (2017) 1–48.
[7] Q. Luo, J.D. Li, B. Li, B. Liu, H.Y. Shao, Q. Li, J. Magnes. Alloy. 7 (2019) 58–71.
[8] C.Q. Zhou, Y.Y. Peng, Q.G. Zhang, J. Mater. Sci. Technol. 50 (2020) 178–183.
[9] G.L. Xia, Y.B. Tan, X.W. Chen, D.L. Sun, Z.P. Guo, H.K. Liu, L.Z. Ouyang, M. Zhu, X.B. Yu, Adv. Mater. 27 (2015) 5981–5988.
[10] O. Zavorotynska, A. El-Kharbachi, S. Deledda, B.C. Hauback, Int. J. Hydrog. Energy 41 (2016) 14387–14403.
[11] J.G. Yuan, H.X. Huang, Z. Jiang, Y.J. Lv, B.G. Liu, B. Zhang, Y.H. Yan, Y. Wu, ACS Appl. Nano Mater. 4 (2021) 1604–1612.
[12] Y.J. Lv, Y. Wu, Prog. Nat. Sci. 31 (2021) 809–820.
[13] Y.J. Yang, Y.F. Liu, Y. Li, M.X. Gao, H.G. Pan, J. Phys. Chem. C 117 (2013) 16326–16335.
[14] Y. Li, Y.F. Liu, X. Zhang, Y.X. Yang, M.X. Gao, H.G. Pan, Int. J. Hydrog. Energy 41 (2016) 2788–2796.
[15] Y. Li, Y.F. Liu, X. Zhang, D. Zhou, Y.H. Lu, M.X. Gao, H.G. Pan, J. Mater. Chem. A 4 (2016) 8366–8373.
[16] Y.J. Yang, Y.F. Liu, Y. Li, M.X. Gao, H.G. Pan, Chem.-Asian J. 8 (2013) 476–481.
[17] Y.J. Yang, Y.F. Liu, Y. Zhang, Y. Li, M.X. Gao, H.G. Pan, J. Alloy. Compd. 585 (2014) 674–680.
[18] H.X. Huang, B.G. Liu, Y.J. Lv, W. Lv, J.G. Yuan, Y. Wu, J. Alloy. Compd. 901 (2022) 163468.

[19] Z.W. Tang, H. Chen, X.W. Chen, L.M. Wu, X.B. Yu, J. Am. Chem. Soc. 134 (2012) 5464–5467.
[20] A. Al-Kukhun, H.T. Hwang, A. Varma, Int. J. Hydrog. Energy 37 (2012) 17671–17677.
[21] X.C. Wang, X.Z. Xiao, J.G. Zheng, Int. J. Hydrog. Energy 45 (2020) 2044–2053.
[22] Z.G. Zhang, H. Wang, J.W. Liu, M. Zhu, Thermochim. Acta 560 (2013) 82–88.
[23] J.G. Zheng, X.Z. Xiao, L.T. Zhang, S.Q. Li, H.W. Ge, L.X. Chen, J. Mater. Chem. A 5 (2017) 9723–9732.
[24] X.L. Feng, J.G. Yuan, Y.J. Lv, B.G. Liu, H.X. Huang, B. Zhang, Y.H. Yan, S.M. Han, Y. Wu, Int. J. Hydrog. Energy 45 (2020) 16654–16662.
[25] Y.J. Yang, Y.F. Liu, Y. Li, M.X. Gao, H.G. Pan, J. Mater. Chem. A 3 (2015) 570–578.
[26] I.L. Jansa, G.N. Kalantzopoulos, K. Nordholm, B.C. Hauback, Molecules 25 (2020) 780.
[27] H.H. Cheng, L.H. Xu, X.L. Fan, X. Huang, J.J. Liu, K. Yan, Y. Zhang, Int. J. Hydrog. Energy 43 (2018) 9705–9712.
[28] C.J. Cheng, M. Chen, X.Z. Xiao, X. Huang, J.G. Zheng, L.X. Chen, J. Phys. Chem. C 122 (2018) 7613–7620.
[29] A. Pighin, B. Coco, H. Troiani, F.J. Castro, G. Urretavizcaya, Int. J. Hydrog. Energy 43 (2018) 7430–7439.
[30] Y. Yin, B. Li, Z.M. Yuan, Y. Qi, Y.H. Zhang, RSC Adv. 8 (2018) 34525–34535.
[31] Y.F. Liu, K. Zhong, K. Luo, M.X. Gao, H.G. Pan, Q.D. Wang, J. Am. Chem. Soc. 131 (2009) 1862–1870.
[32] X.C. Wang, X.Z. Xiao, J.G. Zheng, Z.M. Hang, W.P. Lin, Z.D. Yao, M. Zhang, L.X. Chen, Int. J. Hydrog. Energy 46 (2021) 23737–23747.
[33] G. Soloveichik, J.H. Her, P.W. Stephens, Y. Gao, J. Rijssenbeek, M. Andrus, J.C. Zhao, Inorg. Chem. 47 (2008) 4290–4298.
[34] F. Yuan, X.W. Chen, Q.F. Gu, Z.W. Tang, X.B. Yu, Int. J. Hydrog. Energy 38 (2013) 5322–5329.
[35] Y.J. Yang, Y.F. Liu, H. Wu, W. Zhou, M.X. Gao, H.G. Pan, Phys. Chem. Chem. Phys. 16 (2014) 135–143.
[36] L.H. Jepsen, M.B. Ley, Y. Filinchuk, F. Besenbacher, T.R. Jensen, ChemSusChem 8 (2015) 1452–1463.
[37] D.P. Kim, K.T. Moon, J.G. Kho, J. Economy, C. Gervais, F. Babonneau, Polym. Adv. Technol. 10 (1999) 702–712.
[38] Z. Li, M. Gao, J. Gu, K.C. Xian, Z.H. Yao, C.X. Shang, Y.F. Liu, Z.X. Guo, H.G. Pan, ACS Appl. Mater. Interfaces 12 (2020) 893–903.
[39] Y.H. Guo, H. Wu, W. Zhou, X.B. Yu, J. Am. Chem. Soc. 133 (2011) 4690–4693.
[40] F. Yuan, Q.F. Gu, Y.H. Guo, W.W. Sun, X.W. Chen, X.B. Yu, J. Mater. Chem. 22 (2012) 1061–1068.
[41] X.W. Chen, X.B. Yu, J. Phys. Chem. C 116 (2012) 11900–11906.
[42] Y.H. Guo, X.B. Yu, W.W. Sun, D.L. Sun, W.N. Yang, Angew. Chem.-Int. Edit. 123 (2011) 1119–1123.
[43] W. Zhu, L. Ren, C. Lu, H. Xu, F.Z. Sun, Z.W. Ma, J.X. Zou, ACS Nano 15 (2021) 18494–18504.
[44] C. Lu, Y.L. Ma, F. Li, H. Zhu, X.Q. Zeng, W.J. Ding, T. Deng, J.B. Wu, J.X. Zou, J. Mater. Chem. A 7 (2019) 14629–14637.